Nakata, K; Ota, K; Ito, S; Ishihara, K; Goto, K; Itouyama, N; Watanabe, H; Kawasaki, A; Matsuoka, K; Kasahara, J; Matsuo, A; Funaki, I; Higashino, K; Braun, J; Meyer, T; Paniagua, G Supersonic Exhaust from a Rotating Detonation Engine with Throatless Diverging Channel AIAA JOURNAL, 60, 7, 2022, 4015-4023

Supersonic Exhaust from a Rotating Detonation Engine with Throatless Diverging Channel

Kotaro Nakata[1], Kosei Ota[1], Shiro Ito[1], Kazuki Ishihara[1], Keisuke Goto[2], Noboru Itouyama[2], Hiroaki Watanabe[3], Akira Kawasaki[3], Ken Matsuoka[4], and Jiro Kasahara[5]
Nagoya University, Nagoya, 464-8603, Japan

Akiko Matsuo[6]
Keio University, Yokohama, 223-8522, Japan

Ikkoh Funaki[7]
JAXA Institute of Space and Astronautical Science Sagamihara, 252-5210, Japan

Kazuyuki Higashino[8]
Nets Co., Ltd, Sakado, 350-0233, Japan

and
James Braun[9], Terrence Meyer[10], and Guillermo Paniagua[10]
Purdue University, West Lafayette, IN47907, USA

Converging-diverging nozzles are common in rocket engine systems to increase the exhaust velocity and improve thrust performance. In this study, we focused on the acceleration of subsonic burned gas without a structural throat via detonation to realize a simple and compact engine. We developed and tested a rotating detonation engine (RDE) without a throat and with a diverging channel (constant diverging angle $\alpha = 5$ deg). Gaseous C_2H_4 and O_2 were used as the propellants, and the mass flow rate ranged from 62–134 g/s in the combustion tests under low back-pressure conditions. We measured pressure and thrust, as well as high-speed

Presented as Paper 2021-3657, "Experimental Study on Truncated Conical Rotating Detonation Engines with Diverging Flows" at the AIAA Propulsion and Energy 2021 Forum, VIRTUAL EVENT, 9-11 August 2021.
[1] Graduate Student, Department of Aerospace Engineering, Aichi.
[2] Designated Assistant Professor, Institute of Materials and Systems for Sustainability, Aichi.
[3] Assistant Professor, Department of Aerospace Engineering, Aichi, Member AIAA.
[4] Associate Professor, Department of Aerospace Engineering, Aichi, Member AIAA.
[5] Professor, Department of Aerospace Engineering, Aichi, Associate Fellow AIAA.
[6] Professor, Department of Mechanical Engineering, Kanagawa, Senior Member AIAA.
[7] Associate Professor, Institute of Space and Astronautical Science, Kanagawa, Senior Member AIAA.
[8] Director, Technical Development Division, Saitama, Member AIAA.
[9] Research Assistant Professor, School of Mechanical Engineering, West Lafayette.
[10] Professor, School of Mechanical Engineering, West Lafayette, Associate Fellow AIAA.

imaging of self-luminescence of the combustion and imaging of the exhaust plume. The pressure at the exit was less than one-fifth of the maximum pressure in the RDE, significantly below the value for a sonic flow. The results suggested that the exhaust flow was supersonic, with values up to Mach 1.7, without the need of a converging section within the engine. In addition to the estimated Mach number from the measured pressure, the exhaust plume images coherently indicated the existence of supersonic exhaust.

Nomenclature

(Nomenclature entries should have the units identified)

A = cross sectional area

d = diameter

F = thrust

g = gravitational acceleration

h = enthalpy

l = length of the first shock cell

L = length of the RDE

m = molecular weight

$\dot{m}$ = mass flow rate

M = axial Mach number

p = pressure

Q = heating value

r = radius

S = area of the side wall of the engine

t = time coordinate

T = temperature

z = axial position in the RDE

α = diverging angle

γ = specific heat ratio

ε = expansion ratio

ϕ = equivalence ratio

Subscripts

b = background

e = exit

E = estimated from exhaust plume

f = fuel

i = indication of axial position ($i = 5$, 10, 20, 30, 40, 60, 65 mm)

inj = injector

ori = orifice

ox = oxidizer

P = estimated from measured pressure

ple = plenum

tank = propellant gas tank

I. Introduction

Accerelation of the burned gas is one of the most important elements for thrust generation of propulsive systems. Deflagration combustion is widely used in chemical rocket engines, operating through material diffusion and heat transfer with a combustion wave that propagates at subsonic speed. Some distance is required to complete the combustion. Because the heat released in the combustion is distributed over some distance, the burned gas cannot be thermally choked. Thus, a converging section is required to achieve supersonic flows in conventional rocket engines [1]. In detonation combustion, on the other hand, the combustion process is continuously triggered by a shock wave leading a combustion wave. The combustion process completes instantly through the supersonic wave [2-5], enabling engine downsizing. Furthermore, when the heat value from the combustion is sufficiently large, and the combustion completion distance is suitably short, the flow of the burned gas can satisfy the choking condition even if the channel is diverging [6]. Thermal choking in a diverging channel enables more flexible design of engine shape, in turn broadening the application option of the engines.

Thermal choking is widely known, especially in Ramjet or Scramjet combustion systems [7]. In these systems, thermal choking is regarded as a problematic phenomenon, because adding heat to the supersonic flow decelerates it, causing unstart. Thus, restricting the heat value of the combustion or balancing it according to the channel geometry is necessary in such systems. As described above, due to the limited combustion speed in deflagrative combustors, heat cannot be employed to accelerate the burned gas, but rather to produce high-temperature, high-pressure gas. Therefore, few studies beyond that by Knuth et al. [8] have focused on acceleration by heat addition. Knuth et al. [8] demonstrated the theoretical feasibility of a thermally choked combustor for a simpler and smaller rocket engine using gaseous H_2 and O_2 as propellants. They used these gases because their high burning velocity enabled the subsonic flow to be thermally choked in the diverging nozzle. However, as already mentioned, a detonation engine can realize this phenomenon through the immediate completion of the combustion process, even with gaseous hydrocarbons with a lower burning velocity than gaseous H_2, resulting in a small, simple rocket engine in which the combustion chamber and diverging nozzle are united. In addition to the simplicity and compactness of the engine system, the theoretical thermal efficiency of the detonation cycle is higher than that of the constant pressure cycle [4,5], resulting in a new type of high-performance rocket engine.

The rotating detonation engine (RDE) is one typical styles of detonation engine. Lu and Braun [9], and Anand and Gutmark [10] conducted wide reviews of the recent studies on RDEs. RDEs usually have an annular channel for detonation waves to stably propagate in the circumferential direction, these are called annular RDEs. A number of researchers have studied the effects of changing the combustor geometry and using nozzles in order to improve the performance of annular RDEs [11-17]. Braun et al. numerically demonstrated the feasibility of diverging nozzles to achieve supersonic outflow conditions in RDEs with an inner end wall [11], and employed this high-speed flow to extract power through the magnetohydrodynamic effect [12]. Hansmetzger et al.[13] experimentally investigated the effect of a change in combustor geometry on detonation rotation. Bach et al. [14] studied the dependency of the stagnation pressure of an RDE, one of the indicators of engine performance on combustor geometry. Yetao et al. [15] numerically analyzed the effect of the nozzle on the propulsion performance of RDEs. Fotia et al. [16] and Rankin et al. [17] experimentally tested RDEs with various type of nozzles. However, an annular channel composed of an inner cylinder is thermally isolated, and a disadvantage in terms of weight reduction.

Recently, several researchers have investigated RDEs without an inner cylinder (cylindrical or hollow RDE) [18-23]. Tang et al. [18] numerically demonstrated that detonation waves can continuously propagate in a cylindrical

combustor. Lin et al. [19] experimentally realized stable rotating detonation waves in a cylindrical RDE. Kawasaki et al. [20] examined the effect of inner cylinder diameter on the thrust performance of an RDE. Anand et al. [21] focused on stable operation of a hollow RDE, and suggested several stabilizing elements. Yokoo et al. [22,23] found that the chamber length of a small cylindrical RDE has no effect on thrust performance, and its exhaust flow is sonic at the exit even though the combustor has a uniform cross-sectional area.

A few studies have been conducted on cylindrical RDEs with converging-diverging nozzles [24-26]. Zhang et al. [24] investigated the effects of Laval nozzles and ignition methods on the operability of an RDE without an inner cylinder using gaseous H_2 and gaseous air as propellants. Peng et al. [25] varied the equivalence and contraction ratios of hollow RDEs with nozzles for C_2H_4-air mixture to study the operating domain. Another study concerning the relation between the detonability of the fuel and operating characteristics of a hollow RDE with a nozzle, including operating range and velocity of the propagating waves also conducted by Peng et al. [26] using three types of fuel. These results imply the application of cylindrical RDEs for rocket engines has become ever more feasible.

Motivated by the combustion characteristics of detonation and recent achievements in cylindrical RDEs, this study focuses on the acceleration of the burned gas in a diverging shaped RDE without an inner cylinder (see Fig. 1). We propose and demonstrate an RDE whose channel has a diverging conical shape. Our objective was to demonstrate the acceleration of the subsonic burned gas by heat addition in the diverging channel through the RDE.

II. Experimental setup

A. Rotating detonation engine with simple diverging channel

Figure 1 presents the scheme of the RDE in this study. The diameter of the engine inlet d_0 is 20 mm, and the channel length L is 70 mm. The engine has a constant diverging angle $\alpha = 5$ deg from the inlet, and the exit diameter d_e is 32.3 mm. The area ratio $(\pi d_e^2/4)\ /\ (\pi d_0^2/4)$ is 2.6. Gaseous C_2H_4 and O_2 were used as the propellant and injected via doublet hole injectors. The fuel and oxidizer injectors have 24 holes, each 0.8 mm in diameter. The fuel and oxidizer injectors are at 90 deg angles from each other and arranged in a circle, with the circles for fuel and oxidizer being 15 mm and 9 mm, respectively, in diameter. The thickness of the wall between injector holes is approximately 0.4 mm. We confirmed that there was no apparent change in the injector holes due to combustion by comparing them before and after each test. The pressure sensor ports are located on the injector surface ($z = 0$ mm, p_0) and side wall ($z = 5$, 10, 20, 30, 40, 60, 65 mm, p_5 to p_{65}) of the engine. All of the pressure sensors are 1 kHz

pressure transducers (PAA-23, Kellar Piezoresistive Pressure Transmitter). A gunpowder ignitor was added on the engine via an ignitor port at z = 63 mm.

B. Measurement methods and experimental conditions

Figure 3 presents a schematic of the thrust measurement and visualization setup in a vacuum chamber. Combustion tests were conducted in a 30 m^3 volume vacuum chamber. During combustion, the back pressure was set in the range of 13–20 ± 1 kPa. The RDE was set on a thrust stand inside the vacuum chamber. The thrust stand was pre-loaded, and thrust was measured by a load cell (Aikoh DUD-50K, rating capacity: 500 N). The load cell was calibrated via known weights. The vacuum chamber has windows for visualization. Self-luminescence in the RDE was captured by a high-speed camera (Phantom v2011, Frame Time: 2.3 μs, Exposure: 0.38 μs) set outside of the vacuum chamber, and a color camera (GoPro Hero5) was put inside the vacuum chamber to capture the exhaust plume. The combustion duration was set to 0.5 s for shot 2, and 1.0 s for the other shots.

Table 1 summarizes the experimental conditions and results. The mass flow rate was controlled by the orifices downstream of the high-pressure propellant tanks (tank volume 47 ± 1 L). The pressure in the tanks was high enough to satisfy the choking condition. Thus, the ideal mass flow rate $\dot{m}_{\mathrm{ideal,tank}}$ could be calculated by Eq. (1) from the properties of the tanks:

$$\dot{m}_{\mathrm{ideal,tank}} = \frac{p_{\mathrm{tank}} A_{\mathrm{ori}}}{\sqrt{RT}} \sqrt{\gamma \left(\frac{2}{\gamma+1}\right)^{\frac{\gamma+1}{\gamma-1}}} \tag{1}$$

The actual mass flow rate $\dot{m}_{\mathrm{tank}}$ was calculated by

$$\dot{m}_{\mathrm{tank}} = C_1 \dot{m}_{\mathrm{ideal,tank}}, \tag{2}$$

where C_1 is a mass flow rate coefficient obtained in the calibration tests, where a decrease in the mass of the tank Δm was measured. The actual mass flow rate was calculated using the operational duration of the tank t_{ope}. Therefore, the mass flow rate coefficient C_1 was obtained by

$$C_1 = \frac{\Delta m}{t_{\mathrm{ope}}} \frac{1}{\dot{m}_{\mathrm{ideal,tank}}}. \tag{3}$$

At the same time, the ideal mass flow rate $\dot{m}_{\mathrm{ideal,ple}}$ could be calculated from Eq. (4) using the properties of the plenum,

$$\dot{m}_{\mathrm{ideal,ple}} = \frac{p_{\mathrm{ple}} A_{\mathrm{inj}}}{\sqrt{RT}} \sqrt{\gamma \left(\frac{2}{\gamma+1}\right)^{\frac{\gamma+1}{\gamma-1}}} \tag{4}$$

and the actual mass flow rate was calculated by Eq. (5) where another mass flow rate coefficient C_2 was defined as Eq. (6).

$$\dot{m}_{\mathrm{ple}} = C_2 \dot{m}_{\mathrm{ideal,ple}} \tag{5}$$

$$C_2 = \frac{\Delta m}{t_{\mathrm{ope}}} \frac{1}{\dot{m}_{\mathrm{ideal,ple}}} \tag{6}$$

Theoretically, the mass flow rate from the properties of the tank are as follows: $\dot{m}_{\mathrm{tank}}$ equals the mass flow rate from the properties of the plenum; and $\dot{m}_{\mathrm{ple}}$. However, there were differences between these two values in the experiments. Pressure losses and real gas effects under the high-pressure condition were considered to be the reason for the difference. Therefore, in this study, the mass flow rates $\dot{m}$ were defined by the value of $\dot{m}_{\mathrm{ple}}$, because pressure losses in the supply system were considered to be smaller than the $\dot{m}_{\mathrm{tank}}$ and the lower pressure value resulting in the smaller real gas effect. The error in the mass flow rate was estimated by $\dot{m}_{\mathrm{tank}}$.

The specific impulse ($I_{\mathrm{sp}} = F \,/\, \dot{m}\mathrm{g}$) was calculated from thrust F and mass flow rate $\dot{m}$. The thrust and pressure data were time-averaged sampled from 0.1–0.4 s for a 0.5 s combustion test, and from 0.4–0.7 s for 1.0 s combustion tests.

Table 1. Experimental conditions and summary of results

No.	$\dot{m}$ [g/s]	ϕ [-]	p_{b} [kPa]	F [N]	I_{sp} [sec]	p_5 [kPa]	p_{65} [kPa]
1	62 ± 11	1.3 ± 0.2	14 ± 1	121 ± 4	119 ± 36	208 ± 8	33 ± 2
2	72 ± 9	1.5 ± 0.4	17 ± 1	144 ± 20	205 ± 39	259 ± 11	40 ± 2
3	78 ± 11	1.5 ± 0.4	15 ± 1	158 ± 6	206 ± 30	300 ± 10	46 ± 2
4	89 ± 9	1.6 ± 0.3	18 ± 1	182 ± 7	207 ± 21	351 ± 8	54 ± 2
5	105 ± 12	1.6 ± 0.4	20 ± 1	216 ± 10	209 ± 25	413 ± 9	67 ± 2
6	108 ± 9	1.7 ± 0.3	19 ± 1	221 ± 9	209 ± 20	421 ± 11	67 ± 2
7	126 ± 16	1.6 ± 0.2	13 ± 1	277 ± 5	224 ± 29	521 ± 30	83 ± 1
8	134 ± 15	1.4 ± 0.2	16 ± 1	295 ± 14	224 ± 28	555 ± 8	87 ± 1

III. Results and Discussion.

A. Combustion mode

Figure 4 contains a typical axial image of self-luminescence in the RDE. The focus plane was manually adjusted to the injector surface. In the combustion tests, the propagation of the high-luminescence area was observed for the combustion duration at constant speed, except for the smallest mass flow rate condition ($\dot{m} = 62$ g/s), in which oscillations in the axial direction were observed in the high-luminescence area. When the mass flow rate ranged from 72–89 g/s, axial oscillation was occasionally observed, but no oscillation was observed when the rate was 105 g/s or

more. The differences between time-averaged pressure value and thrust performance from test cases in which the axial oscillations were observed and those without oscillations could not be recognized in this study. Thus, measured data were analyzed without distinguishing the combustion mode.

The velocity of the propagating high-luminescence area was approximately 1200 m/s at $d = 15$ mm. The velocity was 44–49% of the C-J detonation velocity calculated by the NASA-CEA [27] detonation mode using pressure p_5, equivalence ratio ϕ, and room temperature as the initial condition. From the perspective of angular velocity, the propagating high-luminescence area was approximately 1.6×10^5 rad/s in this study. This was calculated based on the averaged value within 10 arbitrary revolutions using the pictures captured by the high-speed camera. The angular velocities were slightly less than those in a previous study by Yokoo et al.[22] for a straight channel with angular velocities (approximately 1.6×10^5 to 1.8×10^5 rad/s). Thus, the propagating high-luminescence area in the diverging RDE was detonation combustion. Detonation wave propagation at a velocity less than C-J speed was due to several differences between the ideal conditions and actual experiment conditions, such as channel radius and insufficient mixing of the propellant [21,23].

B. Pressure distribution and thrust

Figure 5 presents an example of typical variation of pressure and thrust. The plenum pressure values were steady just before ignition and during the combustion. The steady pressure value in the plenum means that injection conditions did not change before and after ignition. Figure 6 shows the time-averaged axial pressure distribution for all test cases. In all combustion tests, the maximum pressure value was p_5, and pressure then decreased according to the axial position. The pressure ratio between the maximum pressure in the engine p_5 and the pressure at the vicinity of the exit p_{65} was approximately 0.16 for all test cases. It is difficult to measure or estimate the actual value of stagnation pressure p_c via the pressure sensor for p_0, because there is a velocity component around the p_0 pressure port due to the orthogonal or circumferential flow around the port. The main cause of the flow was considered to be the high-speed flow of propellants injected from the holes around pressure port for p_0 (see Fig. 1). Although the propellants were not mixed well in the initial region of the engine, the effect of the heat release was limited, and the diverging effect in the subsonic region contributed to the pressure rise, the effect was estimated to be limited considering the cross-sectional area ratio. Therefore, the main cause of the increased pressure from p_0 to p_5 was thought to be the high-speed flow around the pressure port.

The thrust of an RDE can be estimated by using control surface theory [23]. We calculated the thrust based on the theory to validate the thrust measured by load cell. For these calculations, we disregarded the gravitational and viscous forces. When the control surface was set on the RDE along the engine wall (see Fig. 7), the pressure loaded on the inner side wall contributed to generate thrust. Total thrust from the RDE was composed of the moment of the injected propellants and pressure on the injector surface, inner side wall and outer wall of the RDE. The total thrust $F_{\mathrm{cs}} = (F_{\mathrm{m}} + F_{\mathrm{p}})$ was defined as the sum of the momentum thrust F_{m} and the pressure thrust F_{p}.

The momentum thrust F_{m} can be obtained from

$$F_{\mathrm{m}} = \left(\dot{m}_{\mathrm{ox}} v_{\mathrm{inj,ox}} + \dot{m}_{\mathrm{f}} v_{\mathrm{inj,f}}\right) \cos 45^{\circ}, \tag{7}$$

using the mass flow rate $\dot{m}$ in Eq. (5). The injection speed v_{inj} was assumed to be sonic calculated by Eq. (8) and the velocity vector tilted 45 deg to the z-axis (see Fig. 7):

$$v_{\mathrm{inj}} = \sqrt{\frac{2\gamma}{\gamma - 1} RT}. \tag{8}$$

The pressure thrust F_{p} is expressed as follows (see Fig. 7):

$$F_{\mathrm{p}} = p_{\mathrm{inj,ox}} A_{\mathrm{inj,ox}} + p_{\mathrm{inj,f}} A_{\mathrm{inj,f}} + p_0 (A_0 - A_{\mathrm{inj,ox}} - A_{\mathrm{inj,f}}) + \int_S p_i dS \sin\alpha - p_{\mathrm{b}} A_{70}, \tag{9}$$

where the pressure at the exit of the injector holes p_{inj} was calculated from

$$p_{\mathrm{inj}} = p_{\mathrm{ple}} \left(\frac{2}{\gamma + 1}\right)^{\frac{\gamma}{\gamma - 1}}, \tag{10}$$

assuming isentropic sonic injection. The inner pressure loaded on the side wall of the engine was integrated using the pressure values from linear interpolation between the measured values.

The total thrusts from the control surface theory F_{cs} were described as Eq. (11):

$$\begin{aligned} F_{\mathrm{cs}} = {} & \left(\dot{m}_{\mathrm{ox}} v_{\mathrm{inj,ox}} + \dot{m}_{\mathrm{f}} v_{\mathrm{inj,f}}\right) \cos 45^{\circ} + p_{\mathrm{inj,ox}} A_{\mathrm{inj,ox}} + p_{\mathrm{inj,f}} A_{\mathrm{inj,f}} \\ & + p_0 (A_0 - A_{\mathrm{inj,ox}} - A_{\mathrm{inj,f}}) + \int_S p_i dS \sin\alpha - p_{\mathrm{b}} A_{70} \end{aligned} \tag{11}$$

In Fig. 8, we compare the estimated thrust using control surface theory F_{cs} and the measured value of the thrust F_{load}. The difference between the estimation and measurement was approximately 3% of the measured value F_{load} in the combustion duration. Thus, the thrust generated from the RDE was considered to be properly measured by the load cell in the configuration used in this study.

C. Acceleration mechanism of the inner flow of the RDE

The inner flow of the RDE was modeled as a quasi-one-dimensional (quasi-1-D) steady flow of calorically perfect gas. The following several assumptions were introduced in this model:

1) Gravitational force and viscous force can be ignored.
2) The combustion process was completed, and all the heat released from the combustion was fed into the flow within a heat-release region.

For an ideal gas, the equation of state is given as follows,

$$p = \rho RT, \tag{12}$$

where ρ is density of the gas, R is the gas constant, and T is gas temperature. The sound of speed is described as Eq. (13),

$$a^2 = \gamma RT, \tag{13}$$

from the definition of the Mach number,

$$M \equiv \frac{u}{a} \tag{14}$$

When gravitational force and viscous force can be ignored, a quasi-1-D steady flow satisfies the continuity equation, momentum equation, and energy equation as follows [6],

$$\frac{1}{\rho}\frac{d\rho}{dz} + \frac{1}{u}\frac{du}{dz} + \frac{1}{A}\frac{dA}{dz} = 0 \tag{15}$$

$$u\frac{du}{dz} + \frac{1}{\rho}\frac{dp}{dz} = 0 \tag{16}$$

$$(\gamma - 1)M^2\frac{1}{u}\frac{du}{dz} - \frac{1}{\rho}\frac{d\rho}{dz} + \frac{1}{p}\frac{dp}{dz} - \frac{1}{h}\frac{dQ}{dz} = 0. \tag{17}$$

The relationship between Mach number, the change in the cross-sectional area dA, and the heating value dQ is obtained as follows using Eqs. (12) - (17).

$$\frac{dM^2}{M^2} = \frac{-[2 + (\gamma - 1)M^2]\left(\frac{dA}{A}\right) + (1 + \gamma M^2)\left(\frac{dQ}{h}\right)}{1 - M^2} \tag{18}$$

Equation (18) clearly indicates the flow at subsonic speed can be accelerated when the heating value fed into the flow dQ is large enough for the increase in the cross-sectional area of the channel dA.

We solved Eqs. (12) - (17) based on the Mach number at the exit by iterative calculation according to the following process. As the first step, an initial pressure in the engine p_0 was assumed to obtain the total heating

value from the combustion Q, initial density ($\rho_0 = p_0/RT_0$), and initial velocity of the flow ($u_0 = \dot{m} / \rho_0 A_0$) in the engine. The initial temperature T_0 was set to the critical temperature of the isentropic sonic flow for the temperature of the experimental room. The total heating value Q was defined as the difference in enthalpy between the unburned and burned gas at the initial temperature. The chemical equilibrium composition of unburned gas was given by equivalence ratio ϕ of the combustion tests, and that of burned gas as that of the C-J states computed by the NASA-CEA detonation mode [27] with the equivalence ratio ϕ, pressure p_0, and temperature of the experimental room. The enthalpy of each of the components were from polynomials given in NASA-CEA [27]. The total heating value Q was obtained from Eq. (19),

$$Q = \left(\sum \mu_{\mathrm{j}} h_{\mathrm{j}(T)}\right)_{\mathrm{unburned}} - \left(\sum \mu_{\mathrm{k}} h_{\mathrm{k}(T)}\right)_{\mathrm{burned}}, \tag{19}$$

where μ_{j} and μ_{k} were the mass fraction of the unburned and burned gas, respectively. The total heating value Q was approximately 5 MJ/kg for all the test cases.

The change in the cross-sectional area dA was known; thus, the amount of heat fed into the flow dQ should be set to solve Eqs. (12) - (17). We assume the heating value generated from combustion was distributed according to the reaction progress variable λ [23] shown in Eq. (20).

$$\lambda = -\frac{z}{l_{\mathrm{heat}}^2}(z - 2l_{\mathrm{heat}}) \quad (z < l_{\mathrm{heat}}) \tag{20}$$

The value of λ reached 1 at $z = l_{\mathrm{heat}}$, and then no reaction or heat addition to the flow occurred. In this model, the specific heat ratio γ and molecular weight m were changed according to the reaction progress variables λ in the heat-release region l_{heat} as an approximation. These values were set as follows:

$$\gamma = (1 - \lambda)\gamma_{\mathrm{unburned}} + \lambda\gamma_{\mathrm{burned}} \tag{21}$$

$$m = (1 - \lambda)m_{\mathrm{unburned}} + \lambda m_{\mathrm{burned}} \tag{22}$$

Iterative calculations for the axial distribution of the flow properties using the conservation law were conducted to compute the same Mach number as the one calculated based on the experimental results. The Mach number at the exit in the experiment could be estimated by the pressure and geometric parameters of the channel. Based on the self-luminescence observation by Yokoo et al. [22], and the combustion characteristics of the detonation combustion, the main part of the combustion is completed in the region near to the inlet of an RDE. Thus, the effect of the chemical reaction on the flow at the vicinity of the exit was limited, and the flow could be treated as an isentropic flow. The Mach number of the isentropic flow is related to the pressure value and the cross-sectional area of the channel.

When the measured pressure value and cross-sectional area at $z = 60$, 65 mm were used, the Mach number of the flow at these positions, M_{60} and M_{65}, respectively, could be calculated by Eqs. (23) and (24).

$$\frac{p_{65}}{p_{60}} = \left[\frac{(\gamma-1)M_{60}^2+2}{(\gamma-1)M_{65}^2+2}\right]^{\frac{\gamma}{\gamma-1}} \tag{23}$$

$$\frac{A_{65}}{A_{60}} = \frac{M_{60}}{M_{65}}\left[\frac{(\gamma-1)M_{65}^2+2}{(\gamma-1)M_{60}^2+2}\right]^{\frac{\gamma+1}{2(\gamma-1)}} \tag{24}$$

From the assumptions above, the Mach number $M_{\mathrm{e,P}}(\approx M_{65})$ ranged from 1.4–1.7. These Mach numbers were used in the calculation for the axial distribution of the flow properties. In the calculation using Eqs. (23) and (24), the Mach number M_{65} had the minimum value (range 1.3–1.5) when the pressure ratio p_{65}/p_{60} had the minimum value considering the uncertainty of the measured data. This result confirmed the existence of supersonic exhaust flow. On the other hand, when the pressure ratio p_{65}/p_{60} had the maximum value, the M_{65} can be a large value, above Mach 2.0. However, such large value did not appear to exist based on the Mach number estimation using the exhaust plume, as discussed in section D. The objective of this estimation was to ensure that supersonic exhaust from the RDE could be demonstrated, and the experimental results suggested that the physically significant uncertainty could be estimated by the difference between time-averaged value and a minimum value. Considering these factors, the uncertainty of the estimated Mach number $M_{\mathrm{e,P}}$ was evaluated via the differences in this study. An image of the inner flow model is shown in Fig. 9.

Through this process, the flow properties according to the axial direction of the RDE can be obtained (see Fig. 10–12). The axial distribution of the reaction progress variables λ is shown in Fig. 10. The length of the heat-release region l_{heat} ranged from 43–66 mm for all test cases. We present the pressure values from the calculations based on the λ and compare them with the experimental results in Fig. 11. The pressure values from both showed the same tendency. Therefore, the inner flow can be expressed by the quasi-1-D flow model. Figure 12 shows the Mach number in the RDE. The axial position of the choking point ranged in $z = 28$–37 mm.

To validate the assumed length of the heat-release region l_{heat}, we conducted visualization from the side of the RDE utilizing an acrylic side wall. This wall had the same geometrical properties as the engine shown in Fig. 1. Self-luminescence of combustion within 60 mm from the injector surface could be visualized, while the rest of the 10-mm long channel, was invisible due to the metal end plate. The combustion duration was set to 0.5 s and back-pressure

during the test was 20 kPa. The mass flow rate was 113 g/s and the equivalence ratio was 1.2. Figure 13 shows the time-averaged self-luminescence during the combustion test. A total of 201 arbitrary consecutive pictures captured in the combustion were averaged to make this picture. Based on Fig. 13, the strong luminescence area, which is considered to be correlated with the heat-release region, was distributed from the vicinity of the injector surface to approximately 20–30 mm from that surface. From the calculation, 80% of the reaction was completed within approximately 24–37 mm from the injector surface, depending on the experimental conditions. By comparing the visualization and calculation results, although the actual length of the heat-release region l_{heat} remains to be determined, we considered the assumed length of l_{heat} in the calculation was similar to the actual value.

In some cases, the reaction progress variables λ did not reach 1 after $z = 60$ mm. This means the flows at the region near to the exit ($z \geq 60$ mm) were not isentropic. However, the reaction progress variables λ was larger than 0.9, and the difference between the specific heat ratio γ at the $z = 60$ mm and at the exit ($z = 70$ mm) was less than 1%. Thus, the assumption of the calculation was considered to be reasonable under the conditions.

D. Estimation of Mach number of the flow at the exit

We now focus on the Mach number of the flow. When the maximum pressure in the RDE is p_5, and the pressure p_{65} can represent the pressure at the exit, the pressure ratio $p_{65}\ /\ p_5$ can be assumed as the indicator of the exit flow condition. The ratio $p_{65}\ /\ p_5$ was approximately 0.16 in all tests. In the quasi-1-D steady flow, the pressure ratio between the initial pressure in the RDE and that at the sonic point was approximately 0.4. Yokoo et al.'s [22,23] measurement of axial pressure distribution suggested the exit flow is sonic for straight channel RDE because the pressure ratios were near to the sonic. Considering the calculated pressure ratio and the previous results for the sonic exhaust flow, the ratio $p_{65}\ /\ p_5$ in the diverging channel RDE suggested the exhaust flow was supersonic.

The Mach number at the exit can be estimated using the shock cell length. Several studies on the relation between the shock cell structure and the Mach number of the flow have been conducted [28-30]. Love et al. [30] suggested semiempirical formulas concerning the relation between the length of the first cell of the shock-train l_1 and the Mach number of the flow $M_{\mathrm{e,E}}$ for under-expanded jets. When the pressure ratio $p_{\mathrm{e}}\ /\ p_{\mathrm{b}}$ is less than approximately 2, the formula is described as follows:

$$\frac{l_1}{d_{\mathrm{e}}} = 1.55\sqrt{M_{\mathrm{e,E}}^2\left(\frac{p_{\mathrm{e}}}{p_{\mathrm{b}}}\right) - 1} - 0.55\sqrt{M_{\mathrm{e,E}}^2 - 1.} \tag{25}$$

When the pressure ratio is more than approximately 2, the formula is described as follows:

$$\frac{l_1}{d_\mathrm{e}} = 1.52\left(\frac{p_\mathrm{e}}{p_\mathrm{b}}\right)^{0.437} + 1.55\left(\sqrt{2M_{\mathrm{e,E}}^2 - 1} - 1\right) - 0.55\sqrt{M_{\mathrm{e,E}}^2 - 1} + 0.5\left[\frac{1}{1.55}\sqrt{\left(\frac{p_\mathrm{e}}{p_\mathrm{b}} - 2\right)\sqrt{M_{\mathrm{e,E}}^2 - 1} - 1}\right] \tag{26}$$

These formulas were created for the flow from a nozzle whose diverging angle at the exit was 0 deg. However, we do not consider that the angle has a significant effect on the length of the first cell of the shock-train when the diverging angle at the exit is small. The Mach number based on the length of the shock train $M_{\mathrm{e,E}}$ ranged from approximately 1.5–1.7 for the combustion tests in which the shock-trains were clearly captured (see Fig. 14 for example). The length of the shock-train was measured using the pictures of a ruler captured from the same angle as the pictures of the exhaust plumes. Figure 15 is a summary of the estimated Mach numbers based on the measured pressure ratio and the cross-sectional area $M_{\mathrm{e,P}}$, and based on the exhaust plume $M_{\mathrm{e,E}}$. These results of the estimation coherently indicated the existence of supersonic flow.

IV. Conclusion

In this study, we focused on the acceleration of subsonic burned gas without a converging section via heat addition. Detonation combustion was used to investigate the possibility of the acceleration, and to demonstrate supersonic exhaust from a throatless diverging channel. An RDE with an inlet diameter of 20 mm, an axial length of 70 mm, and a constant diverging angle of 5 deg was designed and tested. In addition to the pressure and thrust measurement, high-speed imaging for the combustion mode and normal-speed imaging for the exhaust plume were conducted.

The inner flow of the RDE can be treated as a quasi-1-D steady flow. The calculation results suggested that the choking of the flow was realized, because the heat released in the combustion was fed into the flow within a short distance. The flows were choked before 40 mm from the inlet and then accelerated to supersonic speed.

Our results suggested that the exhaust flow of the RDE was supersonic, with exit Mach numbers between 1.4 and 1.7, estimated from the measured pressure and the shape of the exhaust plume. These findings demonstrate that the flow can be choked without a structural converging section and accelerated to supersonic speed in an RDE in which the combustor and the diverging nozzle are unified.

Nakata, K; Ota, K; Ito, S; Ishihara, K; Goto, K; Itouyama, N; Watanabe, H; Kawasaki, A; Matsuoka, K; Kasahara, J; Matsuo, A; Funaki, I; Higashino, K; Braun, J; Meyer, T; Paniagua, G Supersonic Exhaust from a Rotating Detonation Engine with Throatless Diverging Channel AIAA JOURNAL, 60, 7, 2022, 4015-4023

Funding Sources

This study was subsidized by a "Study on Innovative Detonation Propulsion Mechanism", Research and Development Grant Program (Engineering) from the Institute of Space and Astronautical Science, the Aerospace Exploration Agency, by a Grant-in-Aid for Specially Promoted Research (No.19H05464), and by a "Research and Development of an Ultra-High-Thermal-Efficiency Rotating Detonation Engine with Self-Compression Mechanism," Advanced Research Program for Energy and Environmental Technologies, the New Energy and Industrial Technology Development Organization.

Acknowledgments

One of the authors (K. Higashino) is thankful to AOARD for their partial support by the project number of FA2386-21-1-4024. The test piece was manufactured by Nakashima special steel Co., Ltd.

References

[1] Sutton, G. P., and Biblarz, O., *Rocket Propulsion Elements*, 9th ed.,Wiley, New York, 2016.

[2] Fickett, W., and Davis, W. C., *Detonation: Theory and Experiment,* Dover Publications, New York, 2000, Chaps. 2, 3. doi: 10.1017/S0022112001265604.

[3] Law, C. K., *Combustion Physics*, Cambridge University Press, Cambridge, 2006. doi: 10.1017/CBO9780511754517.

[4] Wolanski, P., "Detonative Propulsion," *Proceedings of the Combustion Institute*, Vol. 34, No.1, 2013, pp. 125-158. doi: 10.1016/j.proci.2012.10.005.

[5] Kailasanath, K., "Review of Propulsive Applications of Detonation Waves," *AIAA Journal*, Vol. 38, No. 9, 2000, pp. 1698-1708. https://doi.org/10.2514/2.1156.

[6] Sasoh, A., *Compressible Fluid Dynamics and Shock Waves*, Springer, 2020, Chap.5. doi.org/10.1007/978-981-15-0504-1.

[7] Curran, E. T., Heiser, W. H., and Pratt, D. T., "Fluid phenomenon in scramjet combustion system," *Annual Review of Fluid Mechanics*, Vol.28, No.1, 1996, pp.323-360. https://doi.org/10.1146/annurev.fl.28.010196.001543.

[8] Knuth, W., Goodman, J., and Litchford, R., "Thermally-Choked Combustor Technology," *N96-16952 Center for Space Transportation and Applied Research Fifth Annual Technical Symposium Proceedings*, 1993.

[9] Lu, F. K., Eric M. B., "Rotating Detonation Wave Propulsion: Experimental Challenges, Modeling, and Engine Concepts," *Journal of Propulsion and Power*, Vol. 30 No. 5, 2014, pp. 1125-1142. doi: 10.2514/1.B34802.

Nakata, K; Ota, K; Ito, S; Ishihara, K; Goto, K; Itouyama, N; Watanabe, H; Kawasaki, A; Matsuoka, K; Kasahara, J; Matsuo, A; Funaki, I; Higashino, K; Braun, J; Meyer, T; Paniagua, G Supersonic Exhaust from a Rotating Detonation Engine with Throatless Diverging Channel AIAA JOURNAL, 60, 7, 2022, 4015-4023

[10] Anand, V., and Gutmark, E., "Rotating Detonation Combustors and Their Similarities to Rocket Instabilities," *Progress in Energy and Combustion Science*, Vol. 73, 2019, pp. 182-234. doi: 10.1016/j.pecs.2019.04.001.

[11] Braun J, Saracoglu B.H., Paniagua G., "Unsteady Performance of Rotating Detonation Engines with Different Exhaust Nozzles," *Journal of Propulsion and Power*, Vol. 33, No. 1, 2017. https://doi.org/10.2514/1.B36164.

[12] Braun J., Saracoglu B.H., Magin T., Paniagua G., "One-Dimensional Analysis of the Magnetohydrodynamic Effect in Rotating Detonation Combustors," *AIAA Journal*, Vol. 54, No. 12, 2016. https://doi.org/10.2514/1.J054989 .

[13] Hansmetzger, S., Zitoun, R. and Vidal, P. "A study of continuous rotation modes of detonation in an annular chamber with constant or increasing section," *Shock Waves*, Vol. 28**,** 1065-1078, 2018. https://doi.org/10.1007/s00193-018-0846-9.

[14] Bach, E., Paschereit, C. O., Stathopoilos, P., and Bohon, M. D., "An empirical model for stagnation pressure gain in rotating detonation combustors," *Proceedings of the Combustion Institute*, Vol. 38, 2021, pp. 3807-3814. https://doi.org/10.1016/j.proci.2020.07.071.

[15] Yetao, S., Meng, L., and Jianping, W., "Continuous Detonation Engine and Effects of Different Types of Nozzle on Its Propulsion Performance," *Chinese Journal of Aeronautics*, Vol. 23, 2010, pp. 647-652. https://doi.org/10.1016/S1000-9361(09)60266-1.

[16] Fotia, M. L., Schauer, F., Kaemming, T., and Hoke, J., "Experimental study of the performance of a rotating detonation engine with nozzle." *Journal of Propulsion and Power*, Vol. 32, No. 3, 2016, pp.674-681. https://doi.org/10.2514/1.B35913.

[17] Rankin, B. A., Kaemming, T. A., Theuerkauf, S. W., and Schauer, F. R., "Overview of Performance, Application, and Analysis of Rotating Detonation Engine Technologies," *Journal of Propulsion and Power*, Vol. 33, No. 1, 2017, pp. 131-143. doi: 10.2514/1.B36303.

[18] Tang, X. M., Wang, J. P., and Shao, Y. T. "Three-Dimensional Numerical Investigations of the Rotating Detonation Engine with a Hollow Combustor," *Combustion and Flame*, Vol. 162, No. 4, 2015, pp. 997-1008. doi: 10.1016/j.combustflame.2014.09.023

[19] Lin, W., Zhou, J., Liu, S., and Lin, Z. "An Experimental Study on CH4/O2 Continuously Rotating Detonation Wave in a Hollow Combustion Chamber," *Experimental Thermal and Fluid Science*, Vol. 62, 2015, pp. 122-130. doi: 10.1016/j.expthermflusci.2014.11.017

[20] Kawasaki, A., Inakawa, T., Kasahara, J., Goto, K., Matsuoka, K., Matsuo, A., and Funaki, I., "Critical Condition of Inner Cylinder Radius for Sustaining Rotating Detonation Waves in Rotating Detonation Engine Thruster," *Proceedings of the Combustion Institute*, Vol. 37, No. 3, 2019, pp. 3461-3469. doi: 10.1016/j.proci.2018.07.070.

[21] Anand, V., St. George, A., Farbos de Luzan, C., and Gutmark, E., "Rotating detonation wave mechanics through ethylene-air mixtures in hollow combustors, and implications to high frequency combustion instabilities," *Experimental Thermal and Fluid Science*, Vol. 92, 2018, pp. 314-325. https://doi.org/10.1016/j.expthermflusci.2017.12.004.

Nakata, K; Ota, K; Ito, S; Ishihara, K; Goto, K; Itouyama, N; Watanabe, H; Kawasaki, A; Matsuoka, K; Kasahara, J; Matsuo, A; Funaki, I; Higashino, K; Braun, J; Meyer, T; Paniagua, G Supersonic Exhaust from a Rotating Detonation Engine with Throatless Diverging Channel AIAA JOURNAL, 60, 7, 2022, 4015-4023

[22] Yokoo, R., Goto, K and Kasahara, J., "Experimental Study of Internal Flow Structures in Cylindrical Rotating Detonation Engines," *Proceedings of the Combustion Institute*. https://doi.org/10.1016/j.proci.2020.08.001.

[23] Yokoo, R., Goto, K., Kim, J., Kawasaki, A., Matsuoka, K., Kasahara, J., Matsuo, A., and Funaki, I "Propulsion Performance of cylindrical Rotating Detonation Engine," *AIAA Journal*, Vol. 58, No. 12, 2020, pp. 5107-5116. https://doi.org/10.2514/1.J058322.

[24] Zhang, H., Liu, W., and Liu, S., "Experimental investigations on H_2/air rotating detonation wave in the hollow chamber with Laval nozzle," *International Journal of Hydrogen Energy*, Vol. 42, 2017, pp. 3363-3370, https://doi.org/10.1016/j.ijhydene.2016.12.038.

[25] Peng, H., Liu, W., Liu, S., and Zhang, H., "Experimental investigation on ethylene-air Conituous Rotating Detonation wave in the hollow chamber with Laval nozzle," *Acta Astronautica*, Vol. 151, 2018, pp. 137-145, https://doi.org/10.1016/j.actaastro.2018.06.025.

[26] Peng, H., Liu, W., Liu, S., and Zhang, H., "Hydrogen-air, ethylene-air, and methane-air continuous rotating detonation in the hollow chamber," Energy, Vol. 211, No.15, 2020, https://doi.org/10.1016/j.energy.2020.118598.

[27] Gordon, S., and McBride, B. J., "Computer Program for Calculation of Complex Chemical Equilibrium Compositions and Applications," NASA RP-1311, 1996.

[28] Tam, C. K. W., "The shock-cell structures ad screech tone frequencies of rectangular and non-axisymmetric supersonic jets," *Journal of Sound and Vibration*, Vol. 121, No. 1, 1988, pp. 135-147. doi: 10.1016/S0022-460X(88)80066-X.

[29] D., Munday, E., Gutmark, J. Liu, and K., Kailasanath, "Flow structure and acoustics of supersonic jets from conical convergent-divergent nozzles," *Physics of Fluids*, Vol. 23, No. 11. https://doi.org/10.1063/1.3657824.

[30] Love, E. S., Grigsby, C. E., Lee, L. P., and Wooding, M. J., "Experimental and theoretical studies of axisymmetric free jets," NASA TR-R-6, 1959.

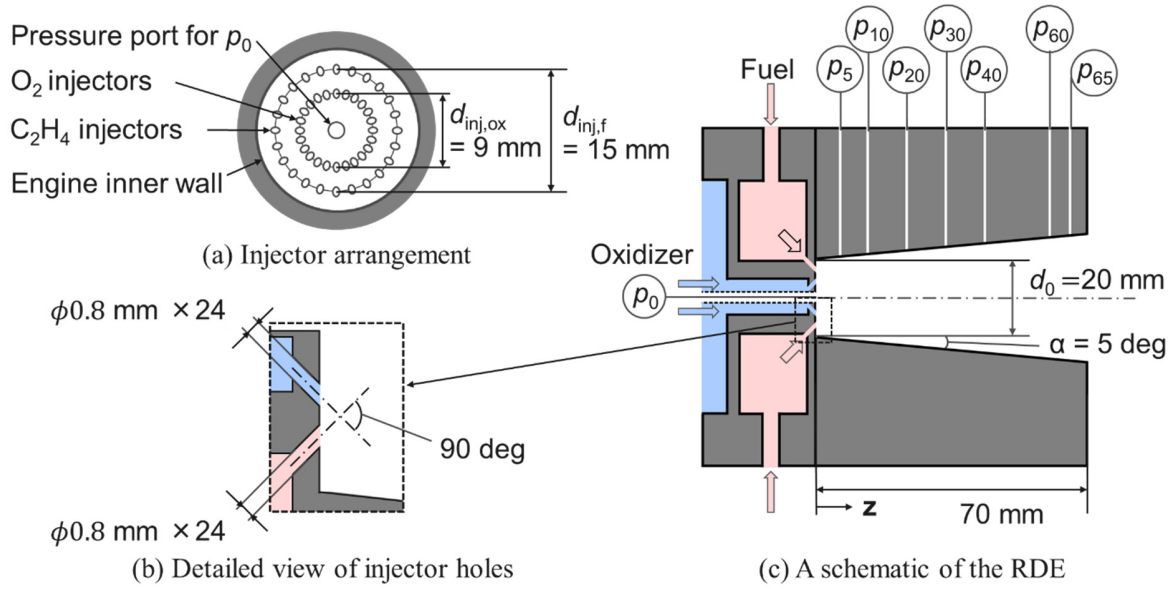

Fig. 1 RDE with simply diverging channel:
(a) Injector arrangement; (b) detailed view of injector holes; (c) schematic of the RDE

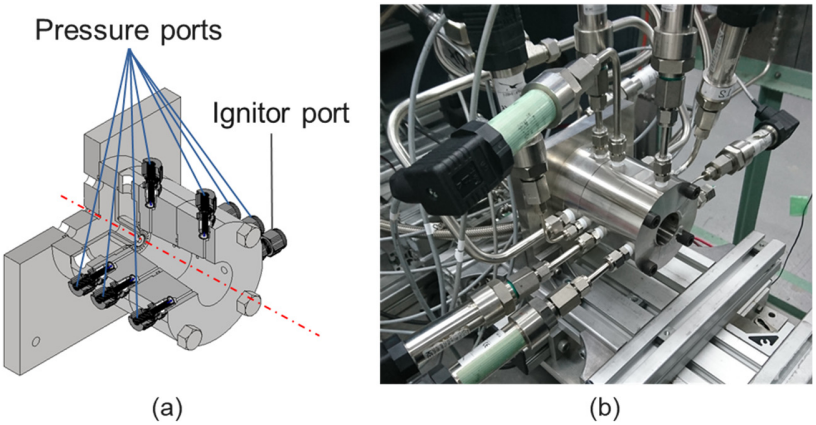

Fig. 2 (a) CAD drawing, and (b) photograph of the RDE
(※ These images are flipped horizontally)

Nakata, K; Ota, K; Ito, S; Ishihara, K; Goto, K; Itouyama, N; Watanabe, H; Kawasaki, A; Matsuoka, K; Kasahara, J; Matsuo, A; Funaki, I; Higashino, K; Braun, J; Meyer, T; Paniagua, G Supersonic Exhaust from a Rotating Detonation Engine with Throatless Diverging Channel AIAA JOURNAL, 60, 7, 2022, 4015-4023

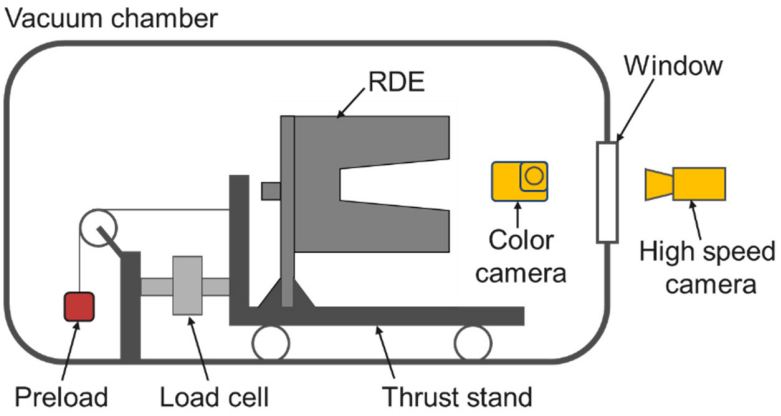

Fig. 3 Schematic of the experimental setup

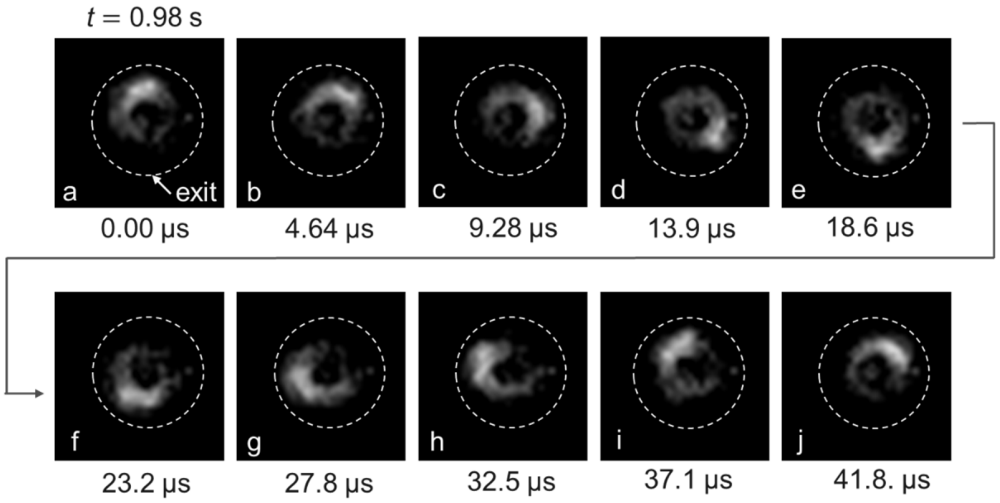

Fig. 4 Axial images of propagating high luminescence area in the RDE ($\dot{m} = 134$ g/s, $= 1.4$, $p_b = 16 \pm 1$ kPa)

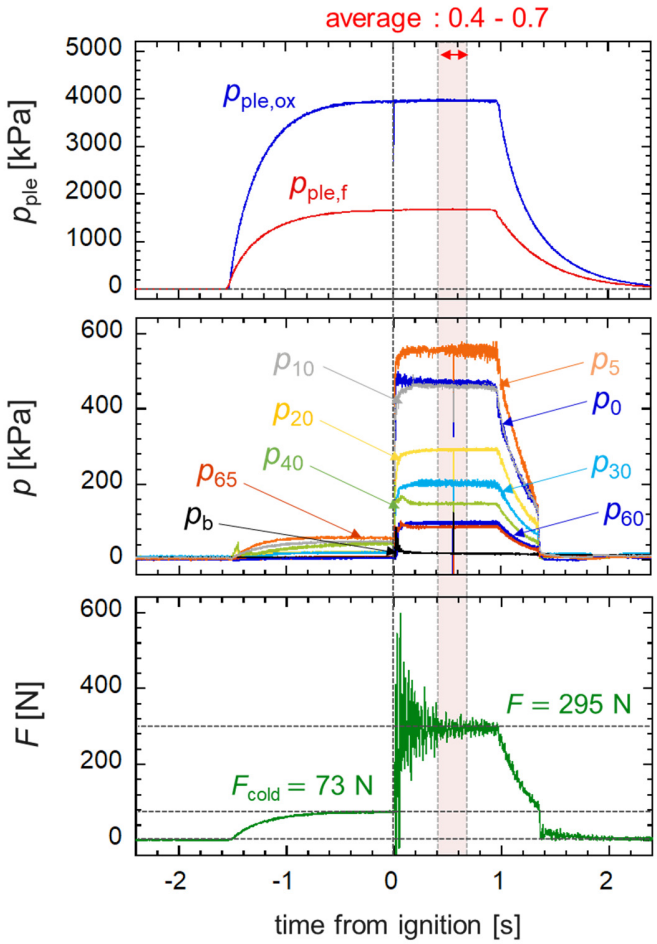

Fig. 5 Time variation of pressure and thrust of the RDE ($\dot{m} = 134$ g/s, $\phi = 1.4$, $p_b = 16 \pm 1$ kPa)

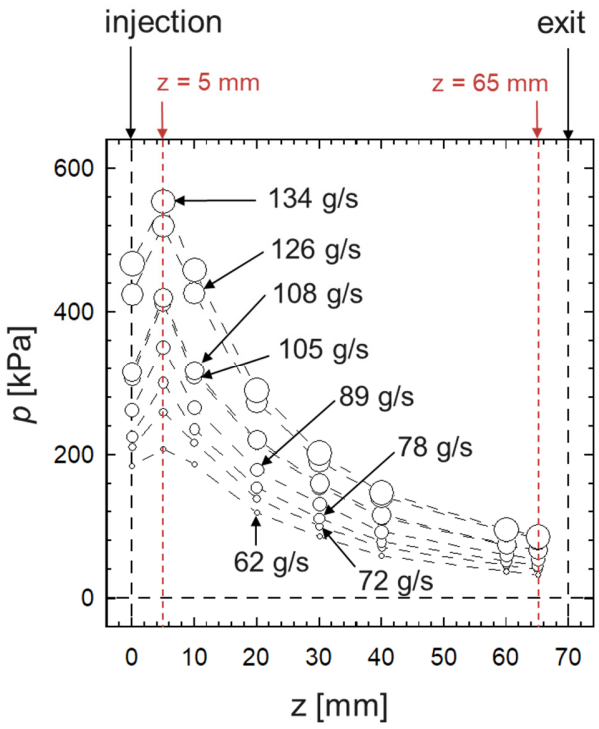

Fig. 6 Time-averaged axial pressure distribution

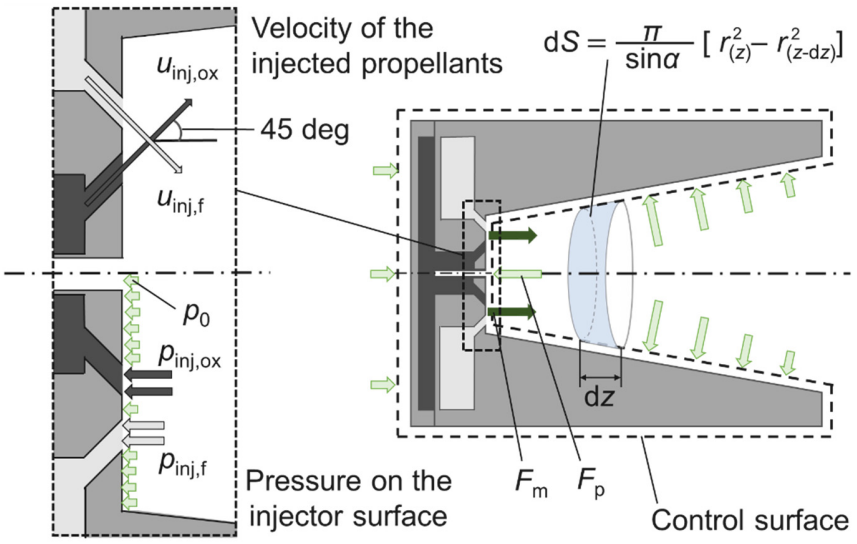

Fig. 7 Scheme of the control surface and assumptions for the estimation of thrust

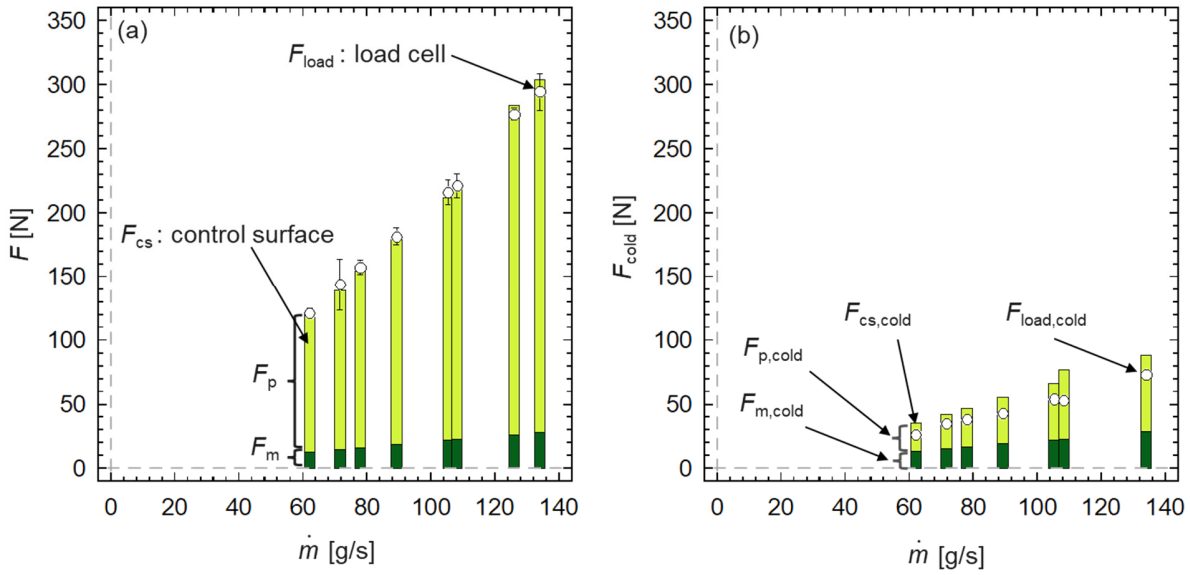

Fig. 8 Comparison of the thrust estimated by control surface theory and that measured by the load cell in the combustion tests (a), and in the cold flow (b)

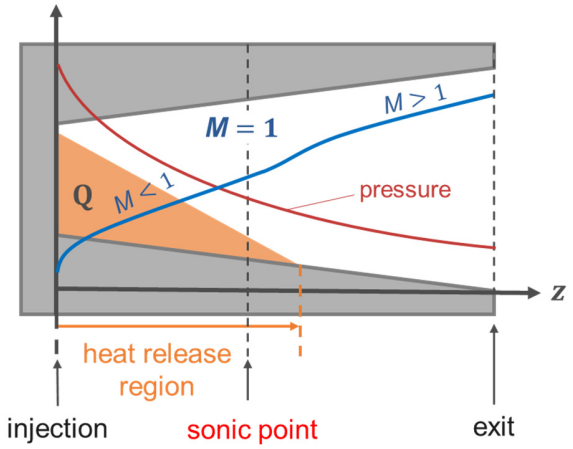

Fig. 9 Image of the inner flow of the RDE

Nakata, K; Ota, K; Ito, S; Ishihara, K; Goto, K; Itouyama, N; Watanabe, H; Kawasaki, A; Matsuoka, K; Kasahara, J; Matsuo, A; Funaki, I; Higashino, K; Braun, J; Meyer, T; Paniagua, G Supersonic Exhaust from a Rotating Detonation Engine with Throatless Diverging Channel AIAA JOURNAL, 60, 7, 2022, 4015-4023

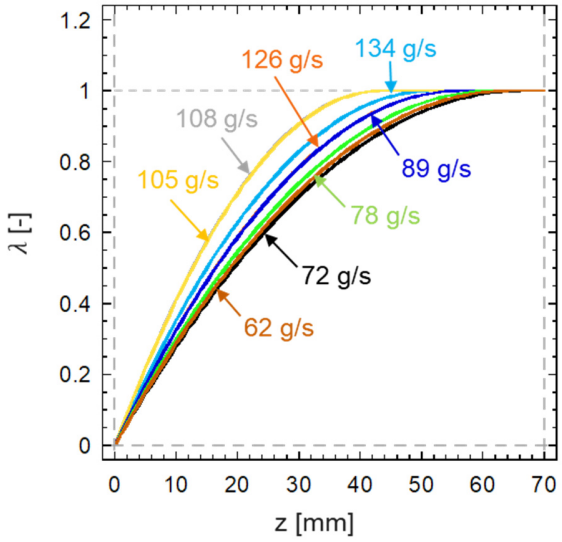

Fig. 10 Axial distribution of the reaction progress variable

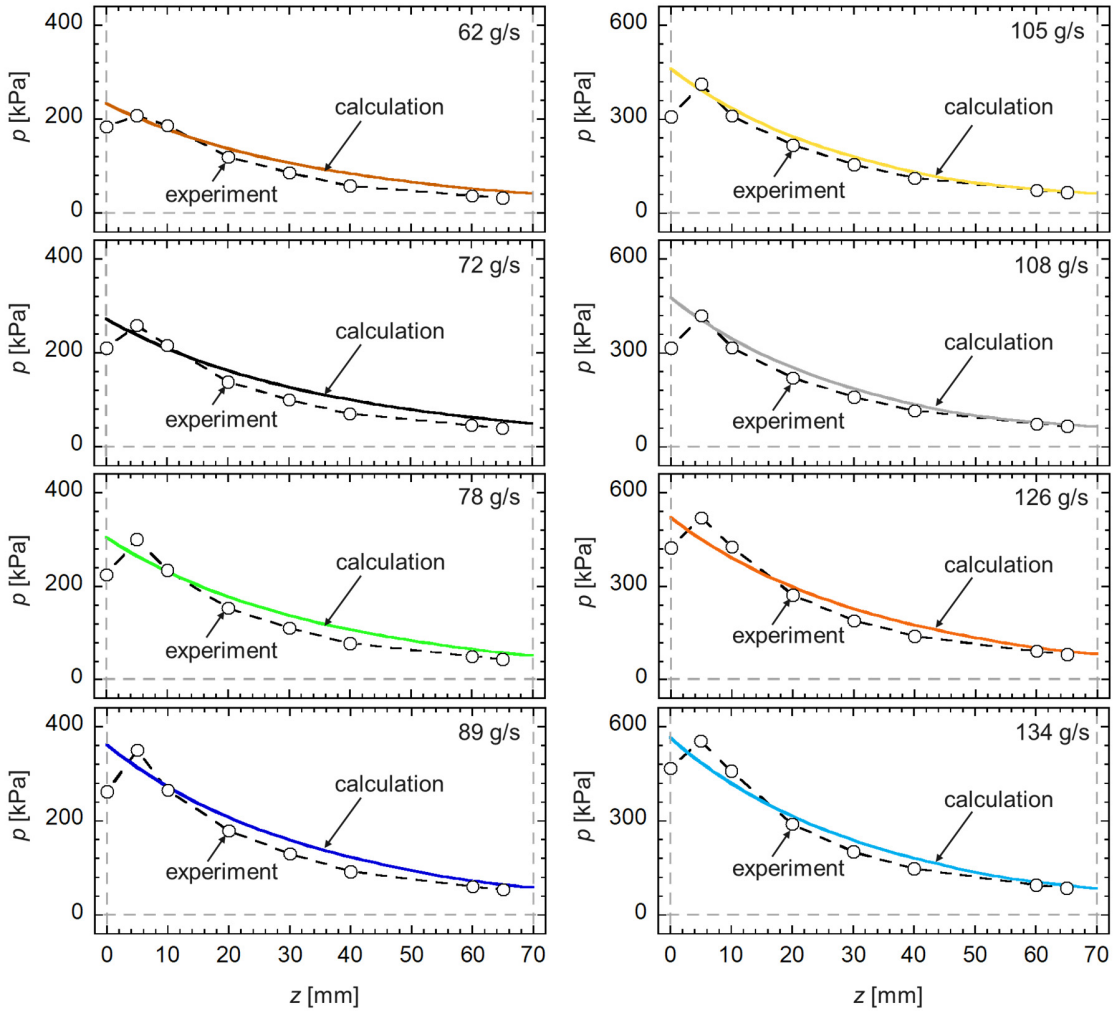

Fig. 11 Axial distribution of the pressure in the RDE

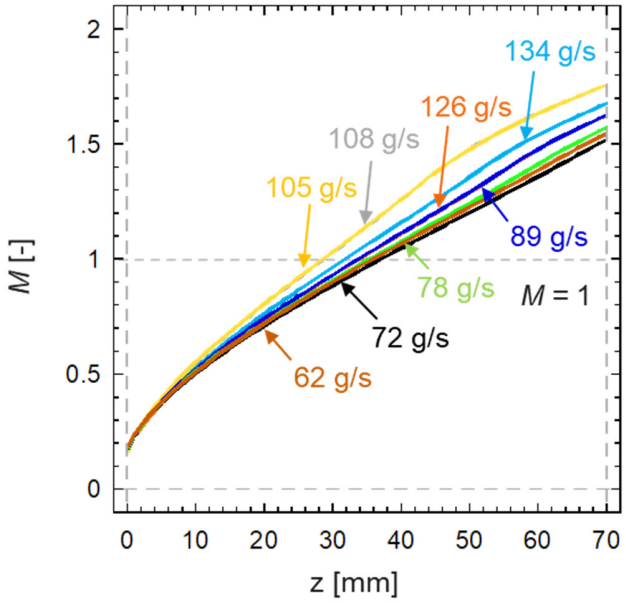

Fig. 12 Axial distribution of the Mach number in the RDE

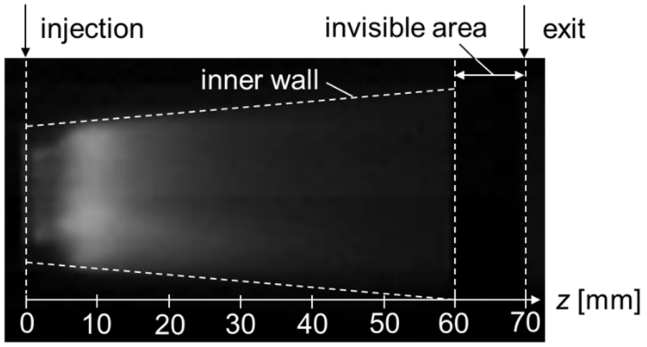

Fig. 13 Time-averaged self-luminescence during combustion ($\dot{m} = 113$ g/s, $\phi = 1.2$, $p_b = 20$ kPa)

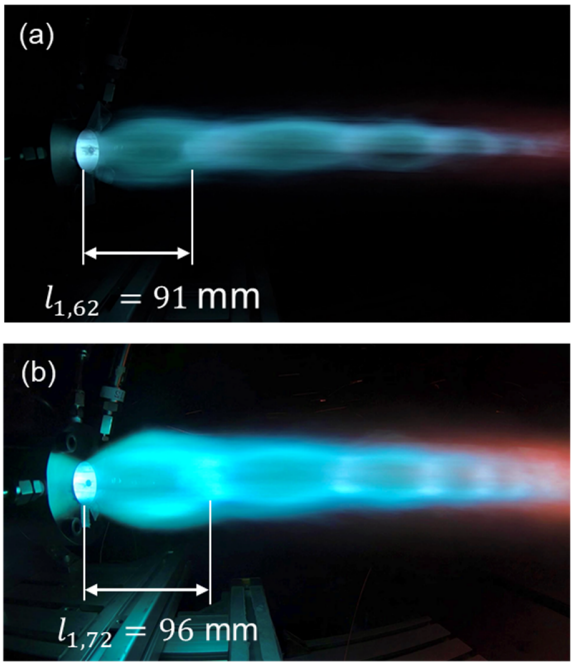

Fig. 14 Shock-cell length for the condition (a) $\dot{m} = 62$ g/s, $\phi = 1.3$, $p_b = 14 \pm 1$ kPa, and (b) $\dot{m} = 72$ g/s, $\phi = 1.5$, $p_b = 17 \pm 1$ kPa (※These images are flipped horizontally)

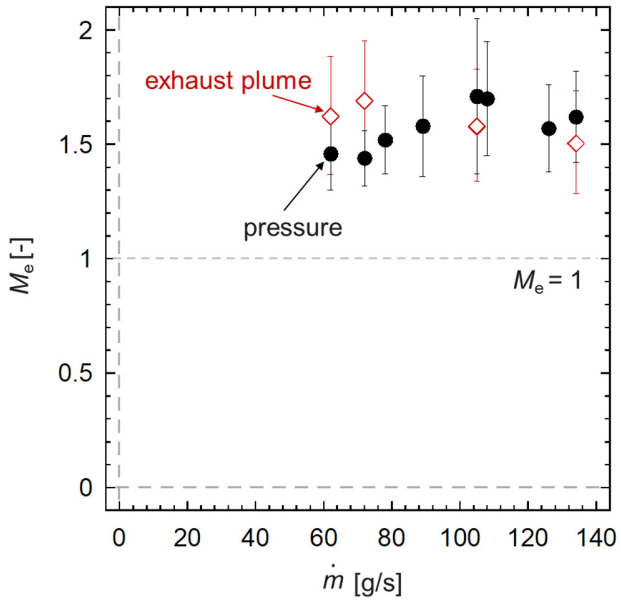

Fig. 15 Mach number estimated by the different proposed methods